CMS AN-2010/XXX

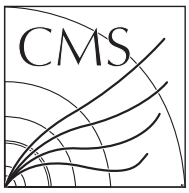

The Compact Muon Solenoid Experiment

Analysis Note

The content of this note is intended for CMS internal use and distribution only

27 Apr 2009

Determination of the $pp \to ZX \to \mu^+\mu^- X$ inclusive cross section with a simultaneous fit of Z yield, muon reconstruction efficiencies and trigger efficiency with the first 2.9 pb^{-1} of 7 TeV collision data

M. De Gruttola, A. De Cosa, F. Fabozzi[a)], L. Lista

INFN Sezione di Napoli, Naples, Italy

Università degli Studi di Napoli "Federico II", Naples, Italy.

D. Piccolo

Laboratori Nazionali INFN di Frascati, Italy.

Abstract

We present the results for the determination of the inclusive cross section of the process $pp \to ZX \to \mu^+\mu^- X$. The method to extract the cross section is based on a simultaneous fit of the yield of $Z \to \mu^+\mu^-$ events, the average reconstruction muon efficiencies in the tracker and in the muon detector, the trigger efficiency, as well as the efficiency of the cut applied to select isolated muons. The extracted Z yield has to be just corrected for the geometrical acceptance and for the integrated luminosity in order to measure the cross section. The measurements obtained with the first 2.9 pb^{-1} is $\sigma(\mathbf{pp \to ZX}) \times \mathbf{BF}(\mathbf{Z \to \mu^+\mu^-}) = \mathbf{0.924 0.031(stat.) 0.022(syst.) 0.101(lumi.) nb}$, in agreement with the Standard Model prediction.

[a)] Also with Università della Basilicata, Potenza, Italy.

Contents

1 Introduction

In the CMS notes [1], [2] and [3] we studied the measurement of the inclusive cross section of the process $pp \to ZX \to \mu^+\mu^- X$ suggesting a way to fit simultaneously the total yield, the muon reconstructions efficiencies, the isolation cut efficiency and the trigger efficiency directly on data, without any estimate of those efficiencies from Monte Carlo (MC). In order to measure the cross section, the Z yield had to be corrected for the trigger efficiency that in Ref. [2] was quoted from the MC truth. In this note we finally apply the strategy on 7 TeV collision data and measure the $Z \to \mu^+\mu^-$ cross-section with a very reduced systematic error.

2 $Z \to \mu^+\mu^-$ cross-section determination

Any physics channel cross-section can be determined from an event counting as

$$\sigma = \frac{N_{sig} - N_{bkg}}{\epsilon \times A \times \mathcal{L}}, \tag{1}$$

where N_{sig} and N_{bkg} are the number of signal and background events passing the selection, ϵ is the efficiency used in the selection, A is the geometrical acceptance, i.e. the fraction of generated events with the selection kinematic cuts (i.e. p_T, —η—), and $\mathcal{L}$ is the machine integrated luminosity.

When the first era of candidates "hunting" was over, two different methods came one after the other to measure the $Z \to \mu^+\mu^-$ cross-section with the first 7 TeV collision data. I personally gave a great contribution to both measurements.

1. The first method is MC driven and has been carried out in the first months of 7 TeV data taking, to achieve a results with the very first few hundred nb^{-1} of data. This method relies on MC expectation to estimate the efficiency values. MC predictions are corrected for remaining differences with respect to data via efficiency correction factors.

2. The second method, is fully data driven, and aims to extract the signal yield and the efficiency terms directly for data using a simultaneous fit to different dimuon categories. This method has been studied in details on simulated data before the collision era and showed to be fully valid with a statistic of a few inverse pb of integrated luminosity.

3 Data driven analysis

A data driven study to determine of the inclusive cross section of the process $pp \to ZX \to \mu^+\mu^- X$ is presented. The method to extract the cross-section is based on a simultaneous fit of the yield of $Z \to \mu^+\mu^-$ events, the average reconstruction muon efficiencies in the tracker and in the muon detector, the trigger efficiency, as well as the efficiency of the cut applied to select isolated muons. The extracted Z yield has to be just corrected for the geometrical acceptance and for the integrated luminosity in order to measure the cross-section. The results are based on a collision data samples of 2.9 pb^{-1}.

3.1 Method description and trigger requirements

The number of produced $Z \to \mu^+\mu^-$ events in a collected data sample can be determined from the number of observed events with two reconstructed isolated global muons having an invariant mass within a range centered at the Z mass peak, corrected by the efficiency of reconstructing the two muons, the trigger selection efficiency, and the efficiency of the isolation cut.

We want to determine both the yield of produced Z events, corrected by the efficiency effects, and the involved efficiency terms from data.

We consider, as muon candidates, global muons, stand alone muons and tracks. We build $Z \to \mu^+\mu^-$ candidates as pairs of muon candidates, and we define the following categories of events with at least one reconstructed $Z \to \mu^+\mu^-$ candidates:

- $Z_{\mu\mu}$: a pair of isolated global muons. This category can be further split into two independent samples:
  - $Z_{\mu\mu}^{\rm 2HLT}$: a pair of isolated global muons, both matched to an HLT trigger object

  - $Z_{\mu\mu}^{\rm 1HLT}$: a pair of isolated global muons only one matched to a trigger object

- $Z_{\mu s}$: a pair of one isolated global muon and one isolated stand-alone muon; the global muon must be matched to a trigger object
- $Z_{\mu t}$: a pair of one isolated global muon and one isolated tracker track; the global muon must be matched to a trigger object.
- $Z_{\mu\mu}^{\rm non\,iso}$: a pair of global muons, where at least one is non isolated; at least one muon must be matched to trigger primitives.

The five categories are explicitly forced to be mutually exclusive in our event selection: if one event falls in the first category it is excluded from the second; if it does not fall in the first category and falls in the second, it is excluded from the third, and so on, in order to have non-overlapping, hence statistically independent, event samples. In case of multiple di-muon candidates for an event falling in one of the categories, all the possible combinations are considered.

We introduce the differential event yields for signal plus background with the following Probability Density Functions (PDF) for each of the four categories:

$$\frac{{\rm d}N_{\mu\mu}}{{\rm d}m} = f_{\mu\mu}(m) = N_{\mu\mu} f_{peak}(m), \tag{2}$$

$$\frac{{\rm d}N_{\mu\mu}^{\rm 2HLT}}{{\rm d}m} = f_{\mu\mu}(m)^{\rm 2HLT} = N_{\mu\mu}^{\rm 2HLT} f_{peak}(m), \tag{3}$$

$$\frac{{\rm d}N_{\mu\mu}^{\rm 1HLT}}{{\rm d}m} = f_{\mu\mu}(m)^{\rm 1HLT} = N_{\mu\mu}^{\rm 1HLT} f_{peak}(m), \tag{4}$$

$$\frac{{\rm d}N_{\mu s}}{{\rm d}m} = f_{\mu s}(m) = N_{\mu s} f_{peak}^{s}(m) + b_{\mu s}(m), \tag{5}$$

$$\frac{{\rm d}N_{\mu t}}{{\rm d}m} = f_{\mu t}(m) = N_{\mu t} f_{peak}(m) + b_{\mu t}(m), \tag{6}$$

$$\frac{{\rm d}N_{\mu\mu}^{\rm non\,iso}}{{\rm d}m} = f_{\mu\mu}^{\rm non\,iso}(m) = N_{\mu\mu}^{\rm non\,iso} f_{peak}(m) + b_{\mu\mu}^{\rm non\,iso}(m). \tag{7}$$

In the above equations, the total signal yield in the different categories is factorized in the terms $N_{\mu\mu} = N_{\mu\mu}^{\rm 2HLT} + N_{\mu\mu}^{\rm 1HLT}$, $N_{\mu s}$, $N_{\mu t}$ and $N_{\mu\mu}^{\rm non\,iso}$, so that the functions $f_{peak}(m)$ and $f_{peak}^{s}(m)$ are normalized to the unity. We have assumed, according to our Monte Carlo estimates, that the background in the samples with two isolated global muons is negligible: we expect $\approx 0.1\%$ of background from non-Z processes, and 0.030% from combinatorial background in Z events producing fake di-muon combinations.

The signal yield in the four categories can be further rewritten in terms of the number of produced $Z \to \mu^+\mu^-$ events, $N_{Z\to\mu^+\mu^-}$, and the average efficiencies for muon reconstruction in the tracker (ϵ_{trk}), in the muon detector as a stand-alone track (ϵ_{sa}), the average efficiency of the isolation cut ($\epsilon_{\rm iso}$) and the average HLT efficiency ($\epsilon_{\rm HLT}$):

$$N_{\mu\mu}^{\rm 2HLT} = N_{Z\to\mu^+\mu^-}\epsilon_{\rm HLT}^2\epsilon_{\rm iso}^2\epsilon_{trk}^2\epsilon_{sa}^2, \tag{8}$$

$$N_{\mu\mu}^{\rm 1HLT} = 2N_{Z\to\mu^+\mu^-}\epsilon_{\rm HLT}(1-\epsilon_{\rm HLT})\epsilon_{\rm iso}^2\epsilon_{trk}^2\epsilon_{sa}^2, \tag{9}$$

$$N_{\mu s} = 2N_{Z\to\mu^+\mu^-}\epsilon_{\rm HLT}\epsilon_{\rm iso}^2\epsilon_{trk}(1-\epsilon_{trk})\epsilon_{sa}^2, \tag{10}$$

$$N_{\mu t} = 2N_{Z\to\mu^+\mu^-}\epsilon_{\rm HLT}\epsilon_{\rm iso}^2\epsilon_{trk}^2\epsilon_{sa}(1-\epsilon_{sa}), \tag{11}$$

$$N_{\mu\mu}^{\rm non\,iso} = N_{Z\to\mu^+\mu^-}(1-(1-\epsilon_{\rm HLT})^2)(1-\epsilon_{\rm iso}^2)\epsilon_{trk}^2\epsilon_{sa}^2. \tag{12}$$

This factorization is done neglecting the correlations between the number of entries in the various categories. This assumption will be justified and discussed in more details in Section 3.2. We can assume that the peak distribution is identical in the categories $Z_{\mu\mu}$, $Z_{\mu t}$ and $Z_{\mu\mu}^{\rm non\,iso}$ becuase the muon momentum resolution in CMS is determined by the tracker measurement for muon with $p_T \leq 200$ GeV, as for the muon from Z decay. We can also neglect the background in the $Z_{\mu\mu}$ category (of the order of few per mille) and we take as distribution for $f_{peak}(m)$ the spectrum of the di-muon invariant mass in the $Z_{\mu\mu}$ category. We have rebinned the distribution in order to match

the bin width in the $Z_{\mu t}$ and $Z_{\mu\mu}^{\text{non iso}}$ categories. In Fig. 1 and 2 we show the level of agreement of the invariant mass distribution for $Z_{\mu\mu}$ candidates selected in signal events with the distributions for $Z_{\mu t}$ and $Z_{\mu\mu}^{\text{non iso}}$ candidates.

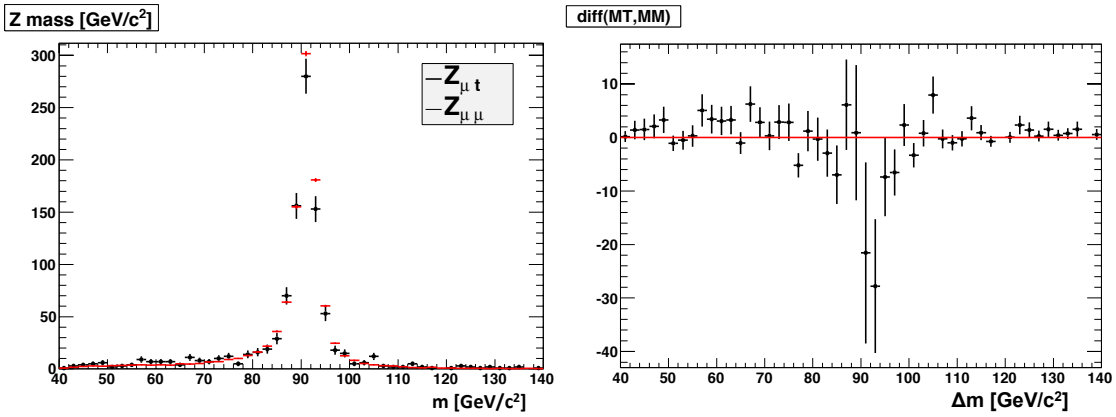

Figure 1: Left: invariant mass distribution for selected $Z_{\mu\mu}$ (red points) and $Z_{\mu t}$ (black points) candidates in signal events. The $Z_{\mu\mu}$ distribution is normalized in order to have the same number of events as the $Z_{\mu t}$ sample. Right: difference between the $Z_{\mu\mu}$ and $Z_{\mu t}$ distributions.

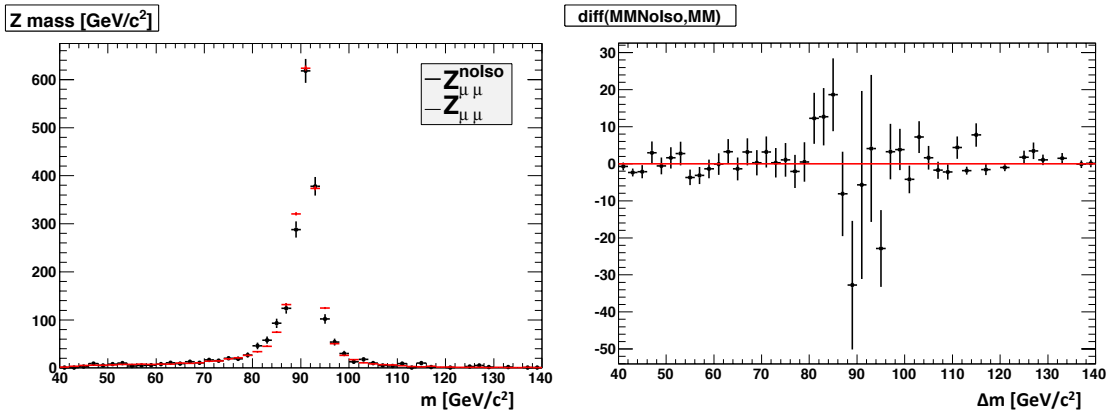

Figure 2: Left: invariant mass distribution for selected $Z_{\mu\mu}$ (red points) and $Z_{\mu\mu}^{\text{non iso}}$ (black points) candidates in signal events. The $Z_{\mu\mu}$ distribution is normalized in order to have the same number of events as the $Z_{\mu\mu}^{\text{non iso}}$ sample. Right: difference between the $Z_{\mu\mu}$ and $Z_{\mu\mu}^{\text{non iso}}$ distributions.

We have also assumed that the isolation efficiency is identical for global muons, tracks and stand-alone muons. For the latter, in particular, the worse direction resolution could produce a slightly different isolation efficiency. We measured on the Monte Carlo signal sample that the difference in isolation efficiency is very small, and compatible with zero within errors:

$$\epsilon_{\text{iso}}^{\text{s.a.}} - \epsilon_{\text{iso}}^{\text{glob.}} = 0.007 \pm 0.057\% \ .$$

In order to determine from data a model for the PDF of the peak function for the $Z_{\mu s}$ category, $f_{peak}^{s}(m)$, we consider the $Z_{\mu\mu}$ candidates, and for one of the muons we take the momentum measured from the muon detector track fit only, in order to mimic a stand-alone muon. We avoid to put the same event twice in the histogram, by choosing alternatively the first (second) muon for even (odd) events respectively. This makes the signal shape description entirely data-driven. Figure 3 compares the invariant mass distribution of the selected $Z_{\mu s}$ candidates with the shape obtained from $Z_{\mu\mu}$ candidates.

Background functions are modeled as products of exponential terms with polynomials of different order for the three samples for which the background is not neglected:

$$b_{\mu t}(m) = N_{\mu t}^{b}(1 + a_1 m + a_2 m^2)e^{-\alpha m} \quad (13)$$

$$b_{\mu\mu}^{\text{non iso}}(m) = N_{\mu\mu}^{b\ \text{non iso}}(1 + b_1 m)e^{-\beta m} \quad (14)$$

$$b_{\mu s}(m) = N_{\mu s}^{b} e^{-\gamma m} \quad (15)$$

With the binned mass values of the five di-muon categories we performe a Poisson likelihood ratio fit[9], minimiz-

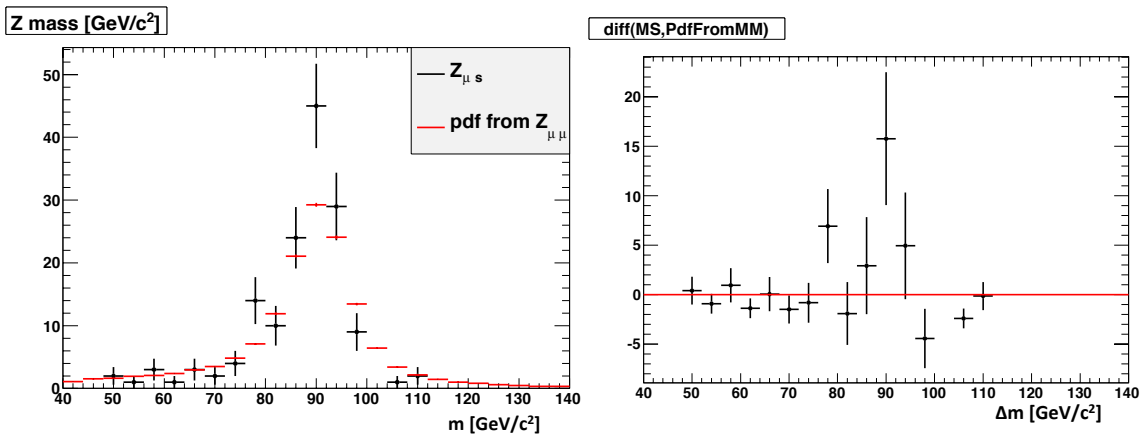

Figure 3: Left: invariant mass distribution for selected $Z_{\mu s}$ candidates in signal events (black points) superimposed to the pdf (red points) determined from $Z_{\mu\mu}$ candidates by using, for one of the muons in the pair, the momentum of the associated stand-alone muon.

ing the function:

$$R = -2\ln\lambda(m) = -2\ln\frac{\text{Poisson}(n_i,\nu_i)}{\text{Poisson}(n_i,n_i)} \tag{16}$$

where ν_i is the expected number of events in the i-bin of the mass histograms and n_i is the measured number of events. For independent Poisson distribution n_i one can demonstrates that that it is equivalent to minimize:

$$R = \sum_{i=1,\ldots 5}\chi^2_{\lambda,i} = 2\sum_{i=i,\ldots,nBins}\nu_i - n_i + n_i\log\frac{n_i}{\nu_i} \tag{17}$$

A benefit of this statistic technique is that it allows a goodness-of-fit test, as for sufficiently large ν_i the minimum of R follows a χ^2 distribution.

So, starting from the 5 independent di-muon categories, the unknown best fit parameters are obtained by minimizing:

$$\begin{aligned} R \;=\; & \frac{(N^{2\text{HLT}}_{\mu\mu} - N_{Z\to\mu^+\mu^-}\epsilon^2_{\text{HLT}}\epsilon^2_{\text{iso}}\epsilon^2_{trk}\epsilon^2_{sa})^2}{N^{2\text{HLT}}_{\mu\mu}} + \\ & \frac{(N^{1\text{HLT}}_{\mu\mu} - 2N_{Z\to\mu^+\mu^-}\epsilon_{\text{HLT}}(1-\epsilon_{\text{HLT}})\epsilon^2_{\text{iso}}\epsilon^2_{trk}\epsilon^2_{sa})^2}{N^{1\text{HLT}}_{\mu\mu}} + \\ & \chi^2_{\lambda,\mu s} + \chi^2_{\lambda,\mu t} + \chi^{\text{non iso }2}_{\lambda,\mu\mu}, \end{aligned}$$

where we count the events $Z^{1\text{HLT}}_{\mu\mu}$ and $Z^{2\text{HLT}}_{\mu\mu}$ golden categories and $\chi^2_{\lambda,\mu s}$, $\chi^2_{\lambda,\mu t}$ and $\chi^{\text{non iso }2}_{\lambda,,\mu\mu}$ are the Poisson likelihood ratio of the di-muon mass binned histograms for the three categories $Z_{\mu s}$, $Z_{\mu t}$, and $Z^{\text{non iso}}_{\mu\mu}$. This technique corrects histograms with 0 entries bin and reduce possible biases with low statistics. The likelihood ration becomes equivalent to simple χ^2 for enough statistics and gives the same statistical errors.

We perform the fit in the range $60 < m < 120$ GeV$/c^2$.

3.2 Correlation studies

In the following sub-sections we consider the possible effect of:

- kinematic correlation between the two muons
- correlation of muon detector reconstruction and HLT efficiency distributions as functions of η and p_T
- correlation of tracker reconstruction and isolation efficiency distributions

3.2.1 Efficiency correlation between the two muons

In the above fit model we assumed that we can factorize the efficiency terms for the two muons (that are products of reconstruction, isolation and trigger efficiencies). We now justify this assumptions, that consists in neglecting the correlation of the efficiency terms, and provide a method to estimate the uncertainty caused by this assumption.

The differential Z yield, as a function of the two muon three-momenta, can be written as:

$$\frac{\mathrm{d}^3 n^0}{\mathrm{d}^3 p_1 \mathrm{d}^3 p_2} = N^0 f_0(\vec{p_1}, \vec{p_2}) \times \epsilon_1(\vec{p_1}) \epsilon_2(\vec{p_2}) \ , \tag{18}$$

where N^0 is the total number of produced events, $\vec{p_1}$ and $\vec{p_2}$ are the two muons three-momenta, $f_0(\vec{p_1}, \vec{p_2})$ is the probability density function that takes into account the process matrix element, phase space, and detector resolutions. We introduce the efficiency terms for the two muons as: $\epsilon_1(\vec{p_1})$, $\epsilon_2(\vec{p_2})$, whose interpretation varies for the different samples we consider. In the case of the sample reconstructed as a pair of global muons, for instance, the two functions ϵ_1 and ϵ_2 coincide, and are equal to the product $\epsilon_{trk}(\vec{p})\epsilon_{sa}(\vec{p})\epsilon_{\mathrm{iso}}(\vec{p})\epsilon_{\mathrm{HLT}}(\vec{p})$.

The differential Z yield as a function of the muon pair invariant mass is:

$$\frac{\mathrm{d}n}{\mathrm{d}m} = N_0 \int \mathrm{d}^3 p_1 \mathrm{d}^3 p_2 f_0(\vec{p_1}, \vec{p_2}) \delta(m_{12}(\vec{p_1}, \vec{p_2}) - m) \epsilon_1(\vec{p_1}) \epsilon_2(\vec{p_2}) \ \ , \tag{19}$$

or sum of similar terms with different $\epsilon_1(\vec{p_1})$ and $\epsilon_2(\vec{p_2})$. The efficiency terms for the other categories are reported in Table 1 for completeness. In the above equation m_{12} is the di-muon invariant mass, which can be writtem as $m_{12} = (\vec{p_1}, \vec{p_2}) = 2p_1p_2(1 - \cos\theta_{12})$ neglecting the muon mass.

$$\frac{\mathrm{d}n^0}{\mathrm{d}m} = N_0 \int \mathrm{d}^3 p_1 \mathrm{d}^3 p_2 f_0(\vec{p_1}, \vec{p_2}) \delta(m_{12}(\vec{p_1}, \vec{p_2}) - m) \ \ , \tag{20}$$

Category	$\epsilon_1(\vec{p_1})$	$\epsilon_2(\vec{p_2})$
$Z_{\mu\mu}^{\mathrm{2HLT}}$	$\epsilon_{trk}(\vec{p_1})\epsilon_{sa}(\vec{p_1})\epsilon_{\mathrm{iso}}(\vec{p_1})\epsilon_{\mathrm{HLT}}(\vec{p_1})$	$\epsilon_{trk}(\vec{p_2})\epsilon_{sa}(\vec{p_2})\epsilon_{\mathrm{iso}}(\vec{p_2})\epsilon_{\mathrm{HLT}}(\vec{p_2})$
$Z_{\mu\mu}^{\mathrm{1HLT}}$	$\epsilon_{trk}(\vec{p_1})\epsilon_{sa}(\vec{p_1})\epsilon_{\mathrm{iso}}(\vec{p_1})\epsilon_{\mathrm{HLT}}(\vec{p_1})$	$\epsilon_{trk}(\vec{p_2})\epsilon_{sa}(\vec{p_2})\epsilon_{\mathrm{iso}}(\vec{p_2})(1-\epsilon_{\mathrm{HLT}}(\vec{p_2}))$
	$\epsilon_{trk}(\vec{p_1})\epsilon_{sa}(\vec{p_1})\epsilon_{\mathrm{iso}}(\vec{p_1})(1-\epsilon_{\mathrm{HLT}}(\vec{p_1}))$	$\epsilon_{trk}(\vec{p_2})\epsilon_{sa}(\vec{p_2})\epsilon_{\mathrm{iso}}(\vec{p_2})\epsilon_{\mathrm{HLT}}(\vec{p_2})$
$Z_{\mu s}$	$\epsilon_{trk}(\vec{p_1})\epsilon_{sa}(\vec{p_1})\epsilon_{\mathrm{iso}}(\vec{p_1})\epsilon_{\mathrm{HLT}}(\vec{p_1})$	$(1-\epsilon_{trk}(\vec{p_2}))\epsilon_{sa}(\vec{p_2})\epsilon_{\mathrm{iso}}(\vec{p_2})$
	$(1-\epsilon_{trk}(\vec{p_1}))\epsilon_{sa}(\vec{p_1})\epsilon_{\mathrm{iso}}(\vec{p_1})$	$\epsilon_{trk}(\vec{p_2})\epsilon_{sa}(\vec{p_2})\epsilon_{\mathrm{iso}}(\vec{p_2})\epsilon_{\mathrm{HLT}}(\vec{p_2})$
$Z_{\mu t}$	$\epsilon_{trk}(\vec{p_1})\epsilon_{sa}(\vec{p_1})\epsilon_{\mathrm{iso}}(\vec{p_1})\epsilon_{\mathrm{HLT}}(\vec{p_1})$	$\epsilon_{trk}(\vec{p_2})(1-\epsilon_{sa}(\vec{p_2}))\epsilon_{\mathrm{iso}}(\vec{p_2})$
	$\epsilon_{trk}(\vec{p_1})(1-\epsilon_{sa}(\vec{p_1}))\epsilon_{\mathrm{iso}}(\vec{p_1})$	$\epsilon_{trk}(\vec{p_2})\epsilon_{sa}(\vec{p_2})\epsilon_{\mathrm{iso}}(\vec{p_2})\epsilon_{\mathrm{HLT}}(\vec{p_2})$
$Z_{\mu\mu}^{\mathrm{non\ iso}}$	$\epsilon_{trk}(\vec{p_1})\epsilon_{sa}(\vec{p_1})\epsilon_{\mathrm{iso}}(\vec{p_1})\epsilon_{\mathrm{HLT}}(\vec{p_1})$	$\epsilon_{trk}(\vec{p_2})\epsilon_{sa}(\vec{p_2})(1-\epsilon_{\mathrm{iso}}(\vec{p_2}))\epsilon_{\mathrm{HLT}}(\vec{p_2})$
	$\epsilon_{trk}(\vec{p_1})\epsilon_{sa}(\vec{p_1})(1-\epsilon_{\mathrm{iso}}(\vec{p_1}))\epsilon_{\mathrm{HLT}}(\vec{p_1})$	$\epsilon_{trk}(\vec{p_2})\epsilon_{sa}(\vec{p_2})\epsilon_{\mathrm{iso}}(\vec{p_2})\epsilon_{\mathrm{HLT}}(\vec{p_2})$
	$\epsilon_{trk}(\vec{p_1})\epsilon_{sa}(\vec{p_1})(1-\epsilon_{\mathrm{iso}}(\vec{p_1}))\epsilon_{\mathrm{HLT}}(\vec{p_1})$	$\epsilon_{trk}(\vec{p_2})\epsilon_{sa}(\vec{p_2})(1-\epsilon_{\mathrm{iso}}(\vec{p_2}))\epsilon_{\mathrm{HLT}}(\vec{p_2})$
	$\epsilon_{trk}(\vec{p_1})\epsilon_{sa}(\vec{p_1})\epsilon_{\mathrm{iso}}(\vec{p_1})\epsilon_{\mathrm{HLT}}(\vec{p_1})$	$\epsilon_{trk}(\vec{p_2})\epsilon_{sa}(\vec{p_2})(1-\epsilon_{\mathrm{iso}}(\vec{p_2}))\epsilon_{\mathrm{HLT}}(\vec{p_2})$
	$\epsilon_{trk}(\vec{p_1})\epsilon_{sa}(\vec{p_1})(1-\epsilon_{\mathrm{iso}}(\vec{p_1}))\epsilon_{\mathrm{HLT}}(\vec{p_1})$	$\epsilon_{trk}(\vec{p_2})\epsilon_{sa}(\vec{p_2})\epsilon_{\mathrm{iso}}(\vec{p_2})(1-\epsilon_{\mathrm{HLT}}(\vec{p_2}))$
	$\epsilon_{trk}(\vec{p_1})\epsilon_{sa}(\vec{p_1})(1-\epsilon_{\mathrm{iso}}(\vec{p_1}))\epsilon_{\mathrm{HLT}}(\vec{p_1})$	$\epsilon_{trk}(\vec{p_2})\epsilon_{sa}(\vec{p_2})(1-\epsilon_{\mathrm{iso}}(\vec{p_2}))(1-\epsilon_{\mathrm{HLT}}(\vec{p_2}))$
	$\epsilon_{trk}(\vec{p_1})\epsilon_{sa}(\vec{p_1})\epsilon_{\mathrm{iso}}(\vec{p_1})(1-\epsilon_{\mathrm{HLT}}(\vec{p_1}))$	$\epsilon_{trk}(\vec{p_2})\epsilon_{sa}(\vec{p_2})(1-\epsilon_{\mathrm{iso}}(\vec{p_2}))\epsilon_{\mathrm{HLT}}(\vec{p_2})$
	$\epsilon_{trk}(\vec{p_1})\epsilon_{sa}(\vec{p_1})(1-\epsilon_{\mathrm{iso}}(\vec{p_1}))(1-\epsilon_{\mathrm{HLT}}(\vec{p_1}))$	$\epsilon_{trk}(\vec{p_2})\epsilon_{sa}(\vec{p_2})\epsilon_{\mathrm{iso}}(\vec{p_2})\epsilon_{\mathrm{HLT}}(\vec{p_2})$
	$\epsilon_{trk}(\vec{p_1})\epsilon_{sa}(\vec{p_1})(1-\epsilon_{\mathrm{iso}}(\vec{p_1}))(1-\epsilon_{\mathrm{HLT}}(\vec{p_1}))$	$\epsilon_{trk}(\vec{p_2})\epsilon_{sa}(\vec{p_2})(1-\epsilon_{\mathrm{iso}}(\vec{p_2}))\epsilon_{\mathrm{HLT}}(\vec{p_2})$

Table 1: List of the efficiency terms to be used in Equation (19) for the different r reconstructed Z categories.

In the fit model above we made the approximation that the efficiency terms can be factorized as average terms $\bar{\epsilon_1}$, $\bar{\epsilon_2}$:

$$\frac{\mathrm{d}n}{\mathrm{d}m} \simeq \frac{\mathrm{d}n'}{\mathrm{d}m} = N_0 \bar{\epsilon_1} \bar{\epsilon_2} \int \mathrm{d}^3 p_1 \mathrm{d}^3 p_2 f_0(\vec{p_1}, \vec{p_2}) \delta(m_{12}(\vec{p_1}, \vec{p_2}) - m) \ , \ . \tag{21}$$

where:

$$\bar{\epsilon_1} \ = \ \langle \epsilon_1(\vec{p_1}) \rangle = \int \mathrm{d}^3 p_1 \mathrm{d}^3 p_2 f_0(\vec{p_1}, \vec{p_2}) \epsilon_1(\vec{p_1}) \ , \tag{22}$$

$$\bar{\epsilon_2} \ = \ \langle \epsilon_2(\vec{p_2}) \rangle = \int \mathrm{d}^3 p_1 \mathrm{d}^3 p_2 f_0(\vec{p_1}, \vec{p_2}) \epsilon_2(\vec{p_2}) \ . \tag{23}$$

The difference between the approximated and exact expressions, due to the normalization of $f(\vec{p_1}, \vec{p_2})$:

$$\int \mathrm{d}^3 p_1 \mathrm{d}^3 p_2 f_0(\vec{p_1}, \vec{p_2}) = 1 \tag{24}$$

is:

$$\frac{\mathrm{d}n}{\mathrm{d}m} - \frac{\mathrm{d}n'}{\mathrm{d}m} = N_0 \int \mathrm{d}^3p_1\mathrm{d}^3p_2 f_0(\vec{p_1},\vec{p_2})\delta(m_{12}(\vec{p_1},\vec{p_2}) - m)(\epsilon_1(\vec{p_1})\epsilon_2(\vec{p_2}) - \bar{\epsilon_1}\bar{\epsilon_2}) \ . \tag{25}$$

Integrating over the mass m, in order to extract the cross-section, in a range $[m_1, m_2]$, one has:

$$N = \int_{m_1}^{m_2} \mathrm{d}m \frac{\mathrm{d}n}{\mathrm{d}m} \ , \tag{26}$$

$$N' = \int_{m_1}^{m_2} \mathrm{d}m \frac{\mathrm{d}n'}{\mathrm{d}m} \ , \tag{27}$$

hence:

$$\begin{aligned} N - N' &= N_0 \int \mathrm{d}^3p_1\mathrm{d}^3p_2 f_0(\vec{p_1},\vec{p_2})(\epsilon_1(\vec{p_1})\epsilon_2(\vec{p_2}) - \bar{\epsilon_1}\bar{\epsilon_2}) \\ &= N_0\langle\epsilon_1(\vec{p_1})\epsilon_2(\vec{p_2}) - \bar{\epsilon_1}\bar{\epsilon_2}\rangle \\ &= N_0\langle(\epsilon_1(\vec{p_1}) - \bar{\epsilon_1})(\epsilon_2(\vec{p_2}) - \bar{\epsilon_2})\rangle \\ &= N_0\mathrm{cov}(\epsilon_1(\vec{p_1}),\epsilon_2(\vec{p_2})) \equiv N_0\mathrm{cov}_{12} \ , \end{aligned}$$

or equivalently:

$$\frac{N - N'}{N_0} = \frac{\Delta N}{N_0} = \mathrm{cov}(\epsilon_1(\vec{p_1}),\epsilon_2(\vec{p_2})) \ . \tag{28}$$

So, the assumption we made is equivalent to neglect the correlation term between the two muon efficiencies, cov_{12}.

Note that the above term is quadratic in the statistical dispersion of the efficiencies in the p_t and η range considered. So, taking two efficiencies for the table 1, if we assume that $\epsilon_k(\vec{p_k}) - \bar{\epsilon_k}$ $(k = 1, 2)$ is at most δ, the relative systematic error introduced by the approximation will be smaller then δ^2. This would give a first way to estimate an upper limit to this systematic effect just looking at the efficiency excursion in the efficiency tables obtained with other method such as the "Tag and Probe" (see Section 3.10 for an explanation of this method) : a 10% dispersion would give a 1% effect.

A more precise way to estimate this effect could be done using the T&P efficiency tables ($\epsilon_k^{tp}(\vec{p})$). We could estimate the needed terms as discrete averages over the signal sample:

$$\bar{\epsilon}_k^{tp} = \frac{1}{N_{\mathrm{obs}}^{\mu,\,k}} \sum_{i=1,\ldots n}^{N_{\mathrm{obs}}^{\mu,\,k}} \epsilon_k^{tp}(\vec{p_i}) \ , \ k = 1, 2 \ , \tag{29}$$

and:

$$\mathrm{cov}_{12}^{tp} = \frac{1}{N_{\mathrm{obs}}^{Z}} \sum_{i=1,\ldots n}^{N_{\mathrm{obs}}^{Z}} (\epsilon_1^{tp}(\vec{p_{1(i)}}) - \bar{\epsilon}_1^{tp})(\epsilon_2^{tp}(\vec{p_{2(i)}}) - \bar{\epsilon}_2^{tp}) \tag{30}$$

$$= \frac{1}{N_{\mathrm{obs}}^{Z}} \sum_{i=1,\ldots n}^{N_{\mathrm{obs}}^{Z}} \epsilon_1^{tp}(\vec{p_{1(i)}})\epsilon_2^{tp}(\vec{p_{2(i)}}) - \bar{\epsilon}_1^{tp}\bar{\epsilon}_2^{tp} \ . \tag{31}$$

Above, N_{obs}^{Z} is the number of observed Z events and is the number of observed muons in Z events for the two category $k = 1,\ 2$ or for the unique category, in case of Z reconstructed from a pair of global muons.

Studies based on MC samples demonstrated that the correlation effect can be neglected at the 0.01% level.

3.2.2 Correlation between trigger efficiency and Reconstruction efficiency

In this section we discuss the correlation between trigger and reconstruction efficiency. This correlation cannot be neglected a-priori and brings to the definition of an effective average trigger efficiency. The trigger efficiency we are considering is indeed the product of the efficiencies L1, L2 and L3 trigger event selection paths.

We rewrite Equation (22) as follows:

$$\bar{\epsilon_i} = \langle \epsilon_i(\vec{p_i}) \rangle = \int \mathrm{d}^3 p_1 \mathrm{d}^3 p_2 f_0(\vec{p_1}, \vec{p_2}) \epsilon_i(\vec{p_i}) \ , i = 1, 2 \ , \tag{32}$$

where $\epsilon_i(\vec{p_i})$, $i = 1, 2$, is one of the terms listed in Table 1. We define for simplicity, omitting the subscript i:

$$\bar{\epsilon} = \langle \epsilon(\vec{p}) \rangle = \int \mathrm{d}^3 p f_0(\vec{p}) \epsilon(\vec{p}) \ , \tag{33}$$

where, for $i = 1$, $f_0(\vec{p_1}) = \int \mathrm{d}^3 p_2 f_0(\vec{p_1}, \vec{p_2})$, and similarly for $i = 2$, $f_0(\vec{p_2}) = \int \mathrm{d}^3 p_1 f_0(\vec{p_1}, \vec{p_2})$.

In the case of the sample reconstructed as a pair of global muons, for instance, the average:

$$\bar{\epsilon} = \langle \epsilon_{trk}(\vec{p}) \epsilon_{sa}(\vec{p}) \epsilon_{\mathrm{iso}}(\vec{p}) \epsilon_{\mathrm{HLT}}(\vec{p}) \rangle \tag{34}$$

does not coincide with the product of the averages: $\langle \epsilon_{trk}(\vec{p}) \rangle \langle \epsilon_{sa}(\vec{p}) \rangle \langle \epsilon_{\mathrm{iso}}(\vec{p}) \rangle \langle \epsilon_{\mathrm{HLT}}(\vec{p}) \rangle$, and again we can assume factorization wherever correlation terms can be neglected. It is reasonable to assume that $\epsilon_{\mathrm{iso}}(\vec{p})$ and $\epsilon_{trk}(\vec{p})$ are uncorrelated w.r.t. the other terms while it could be not the case for $\epsilon_{sa}(\vec{p})$ and $\epsilon_{\mathrm{HLT}}(\vec{p})$, which can be correlated, since single muon trigger is very related to the geometry of the muon detector.

When we express the differential Z yields of the different categories, we have, for each of the two muons, efficiency terms that contain $\epsilon_{sa}(\vec{p})$ and $\epsilon_{\mathrm{HLT}}(\vec{p})$ either as products $\epsilon_{sa}(\vec{p}) \cdot \epsilon_{\mathrm{HLT}}(\vec{p})$, or as single terms containing just $\epsilon_{sa}(\vec{p})$. We never find single terms in $\epsilon_{\mathrm{HLT}}(\vec{p})$. Thus, when we compute the average terms, we are still allowed to use factorization in Equations (8), (9), (10), (11) and (3.4), but we have to re-define ϵ_{HLT} as:

$$\epsilon_{\mathrm{HLT}} = \frac{\langle \epsilon_{sa}(\vec{p}) \cdot \epsilon_{\mathrm{HLT}}(\vec{p}) \rangle}{\langle \epsilon_{sa}(\vec{p}) \rangle} \ , \tag{35}$$

and so we interprete ϵ_{HLT} as the efficiency to trigger a muon which has been correctly reconstructed in the muon system.

3.2.3 Correlation between tracking efficiency and isolation efficiency

A correlation between tracking efficiency and isolation efficiency may occour in case of very bad tracker noise or large event pile-up situation, in which a simultaneous loss of tracker efficiency and isolation power generated by excess of noise in some detector regions could be present.

If we don't neglect this correlation, a similar treatment as it was discussed in Section 3.2.2 can be done. In a similar way, we can re-define an "effective" isolation efficiency, similarly to Eq. (35):

$$\epsilon_{\mathrm{iso}} = \frac{\langle \epsilon_{trk}(\vec{p}) \cdot \epsilon_{\mathrm{iso}}(\vec{p}) \rangle}{\langle \epsilon_{trk}(\vec{p}) \rangle} \ , \tag{36}$$

interpreting ϵ_{iso} as the efficiency of the isolation cut on muon fully reconstructed in the tracking system. All efficiency terms in the definition of Z categories from Equations (8), (9), (11) and (3.4) remain unchanged, but correlation must be taken into account in the efficiency term of the $Z_{\mu s}$ category, in Equation (10). The term, including correlation, is:

$$\begin{aligned} &\langle \epsilon_{trk}(\vec{p_1}) \epsilon_{\mathrm{iso}}(\vec{p_1}) (1 - \epsilon_{trk}(\vec{p_2})) \epsilon_{\mathrm{iso}}(\vec{p_2}) \rangle + \\ &\langle (1 - \epsilon_{trk}(\vec{p_1})) \epsilon_{\mathrm{iso}}(\vec{p_1}) \epsilon_{trk}(\vec{p_2}) \epsilon_{\mathrm{iso}}(\vec{p_2}) \rangle = \\ &\qquad 2 \langle \epsilon_{trk} \epsilon_{\mathrm{iso}} \rangle (\langle \epsilon_{\mathrm{iso}} \rangle - \langle \epsilon_{trk} \epsilon_{\mathrm{iso}} \rangle) \ . \end{aligned}$$

Replacing in the above term:

$$\langle \epsilon_{trk} \epsilon_{\mathrm{iso}} \rangle = \epsilon_{trk} \epsilon_{\mathrm{iso}}$$

$$\langle \epsilon_{\mathrm{iso}} \rangle = \epsilon_{\mathrm{iso}} - \frac{\mathrm{COV}_{trk\,\mathrm{iso}}}{\epsilon_{trk}} = \epsilon_{\mathrm{iso}} \left(1 - \frac{\mathrm{COV}_{trk\,\mathrm{iso}}}{\epsilon_{trk} \epsilon_{\mathrm{iso}}} \right) \ .$$

We can corrected Equations (10) including a possible correlation term:

$$N_{\mu s} = 2 N_{Z \to \mu^+ \mu^-} \epsilon_{\mathrm{HLT}} \epsilon_{\mathrm{iso}}^2 \epsilon_{trk} \epsilon_{sa}^2 \left((1 - \epsilon_{trk}) - \frac{\mathrm{COV}_{trk\,\mathrm{iso}}}{\epsilon_{trk} \epsilon_{\mathrm{iso}}} \right) \ . \tag{37}$$

This correction would only affect the $Z_{\mu s}$ category that is used to determine the tracker efficiency which we expect that, under normal detector operation, would be very close to one. So, we expect this category to be the one with the smallest statistics. A deviation of the number of $Z_{\mu s}$ events would result in a corresponding variation on the tracker inefficiency $(1 - \epsilon_{trk})$, that would result in a much smaller relative variation of ϵ_{trk}, being ϵ_{trk} close to the unity.

If this covariance term would turn out to be significantly different from zero, as alternative, we can drop the isolation request to the stand-alone muon, and this will allow to fully absorb the covariance term into the redefinition of $\epsilon_{\rm iso}$, as done in Section 3.2.2 for $\epsilon_{\rm HLT}$.

Tracker background and event pile-up don't have such a serious impact, especially at low luminosity, to impair dramatically the tracker performance, as in the case of the current measurement described in this work. Anyway, in order to estimate correctly the correlation term under those pessimistic conditions, a realistic estimate would need either a proper simulation of those detector and run conditions, or control samples from real data taken under those conditions. It's important to note that the same effect may also affect othe $Z_{\mu\mu}^{\rm 2HLT}$ r currently used methods to estimate detector efficiencies, such as the Tag and Probe method (see Section 3.10).

3.3 Data samples

The 2010 7 TeV collision data sample used for this analysis (Run2010A) amounts to an integrated luminosity of 2.9 pb^{-1} (see 5 for details on how the luminoisty measurement is done in CMS). We have used the following Monte Carlo samples generated with the standard CMS generator, simulation and reconstruction chain, assuming a center of mass energy of $\sqrt{s} = 7$ TeV with the same detector condition and reconstruction parameter used for the data taking:

- $pp \rightarrow Z/\gamma^* X \rightarrow \mu^+\mu^- X$
- $pp \rightarrow W^{\pm} X \rightarrow \mu^{\pm}\nu_{\mu} X$
- QCD jets events containing at least one muon with $p_t > 15{\rm GeV}/c$
- $t\bar{t}$.
- WZ and WW

The number of events for each MC sample, the product of the NLO cross-section (σ) times the generator kinematic filter efficiency ($\epsilon_{\rm filter}$, i.e. the fraction of generated event witch fall effectively in the kineatic region accessible by the detectors), and the equivalent integrated luminosity ($\int \mathcal{L}{\rm d}t$) are shown in Table 2.

Sample	$\sigma \times \epsilon_{\rm filter}$ (pb)	$\int \mathcal{L}{\rm d}t$ (pb^{-1})
$pp \rightarrow ZX \rightarrow \mu^+\mu^- X (m > 20)$	1686	100
$pp \rightarrow W^+ X \rightarrow \mu^+\nu_{\mu} X$	6152	100
$pp \rightarrow W^- X \rightarrow \mu^-\nu_{\mu} X$	4179	100
QCD jets, muon $p_t > 15$ GeV/c	79688	60
$t\bar{t}$	162	100
$pp \rightarrow ZX \rightarrow \tau^+\tau^- X$	1686	100
WZ	43	537
WW	18	100
ZZ	5.9	100

Table 2: Analyzed MC data samples.

The analyzed samples are first processed through a preselection phase denominated "skimming" where HLT requirements are applied. At skimming level, it is also required the presence of at least two reconstructed muons or one muon plus one tracker track, with $p_T > 15{\rm GeV/c}$. After that, in order to further reduce the data samples, a secondary skim (sub-skim) was run and the a very light output was has been produced.

3.4 Event selection

Events are required to satisfy the single non-isolated muon trigger with a (L3 trigger step) p_T cut of 9 GeV (7 GeV at L1 trigger step) .

Muons used for Z reconstruction are checked for matching with an HLT object (see Sect. 3.10 for the HLT matching requirement used in the different samples of Z candidates and for additional muon trigger efficiencies estimation results with $Z_{\mu\mu}$).

We require that both muon candidates, either global or stand-alone muons, or tracker tracks, must satisfy:

$$p_T > 20 \text{ GeV}/c \text{ , and } |\eta| < 2.1 \text{ .}$$

We perform the fit in the di-muon mass range $60 < m_{\mu^+\mu^-} < 120 \text{ GeV}/c^2$.

We define as isolation variable the sum of the transverse momenta of all tracks within a cone of radius $\Delta R = \sqrt{\Delta\phi^2 + \Delta\eta^2} = 0.3$ plus the sum of the calorimetric deposit in Ecal and Hcal, diveded by the muon momentum itself.

$$I_{rel}^{comb} = \frac{\sum_{\Delta R<0.3} I_{trk} + I_{Ecal} + I_{HCal}}{p_t}. \tag{38}$$

We require:

$$I_{rel}^{comb} < 0.15 \text{ .}$$

Quality cuts to the tracks are applied in order to select a very pure sample. The efficiencies of these additional seelction cuts are includes together with the reconstruction efficiency terms. We require than a tracker track have:

- at least 11 tracker hits (pixel + silicon tracker layers)
- at least 1 pixel hit

The efficiency ϵ_{trk}, which appairs in the equations 8-, is then re-defined as the efficiency to reconstruct a track and the two additional efficiencies $\epsilon_{trk} \rightarrow \epsilon_{trk} \times \epsilon_{\#TrackerHits>10} \times \epsilon_{\#PixelHits>0}$. Events reconstructed as global muon pairs in which one of the two muon does not satisfy these two additional requirements fall in the $Z_{\mu s}$ category. In addition we require that the standalone muon track should have:

- at least 1 muon hit
- at least 2 segments matched to the muon track.

As a consequence ϵ_{sa} is re-defined as the efficiency to reconstruct a standalone track and the two additional efficiencies $\epsilon_{sa} \rightarrow \epsilon_{sa} \times \epsilon_{\#MuonHits>0} \times \epsilon_{\#Matches>1}$. Events reconstructed as global muon pairs in which one of the two muon does not satisfying these two additional requirements fail in the $Z_{\mu t}$ category.

Figures 4 to 8 show the invariant mass distributions of the selected Z candidates for each category considered in the analysis for data and MC scaled to the data luminosity. Table 3 reports the number of selected candidates for data and MC signal and background in the $[60 - 120]$ GeV$/c^2$ mass range. The MC expected numbers of entries in each categories are scaled to the given data luminosity.

sample	$Z_{\mu\mu}$	$Z_{\mu s}$	$Z_{\mu t}$	$Z_{\mu\mu}^{\text{non iso}}$
$Z \rightarrow \mu^+\mu^-$	950 ± 6	12.5 ± 0.6	50.2 ± 1.2	33.3 ± 1.0
$W^{\pm} \rightarrow \mu^{\pm}\nu_{\mu}$	0.03 ± 0.03	0.23 ± 0.08	2.0 ± 0.2	0.55 ± 0.12
$t\bar{t}$	1.3 ± 0.2	0.10 ± 0.06	1.5 ± 0.3	1.9 ± 0.3
QCD	0.05 ± 0.05	0.5 ± 0.2	0.7 ± 0.2	29.6 ± 1.2
$Z \rightarrow \tau^+\tau^-$	0.52 ± 0.12	0.03 ± 0.03	2.6 ± 0.3	No events
WZ	0.72 ± 0.06	0.011 ± 0.007	0.10 ± 0.02	0.06 ± 0.02
WW	0.32 ± 0.09	No events	0.38 ± 0.10	No events
ZZ	0.55 ± 0.13	No events	0.09 ± 0.05	0.06 ± 0.04
data	913	21	75	66

Table 3: Number of candidates expected (MC) and selected (data) in each category with an invariant mass in the range [60-120] GeV$/c^2$ for 2.9 pb^{-1} in data and MC. Here $Z_{\mu\mu} = Z_{\mu\mu}^{\text{1HLT}} + Z_{\mu\mu}^{\text{2HLT}}$. For MC the separate contributions from signal and background processes are shown.

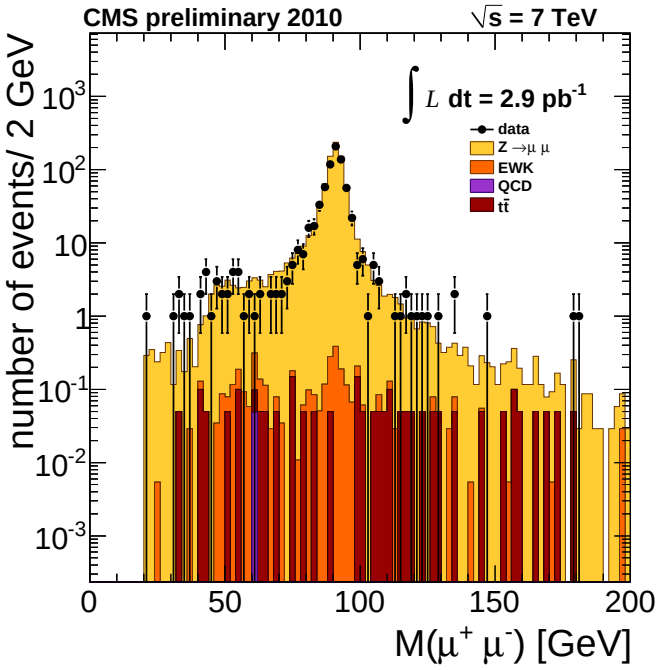

Figure 4: Invariant mass distribution of $Z_{\mu\mu}^{\mathrm{2HLT}}$ candidates for data and MC signal and background events for a luminosity of 2.9 pb^{-1}.

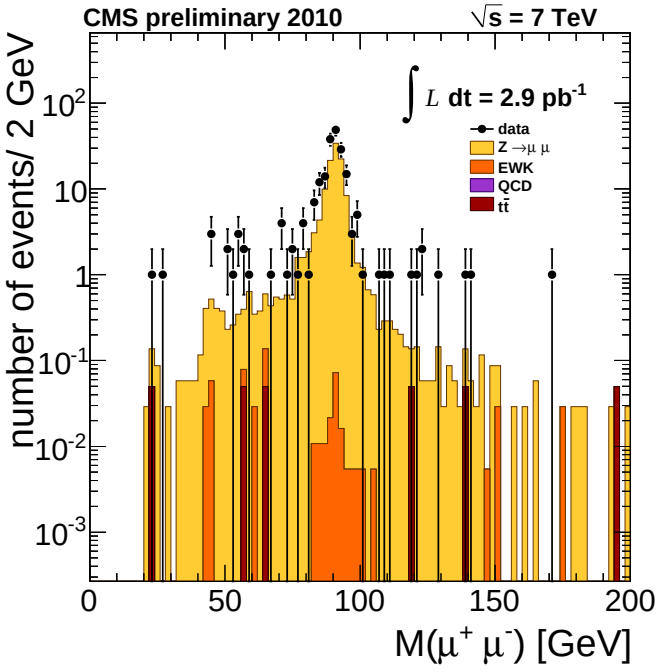

Figure 5: Invariant mass distribution of $Z_{\mu\mu}^{\mathrm{1HLT}}$ candidates for data and MC signal and background events for a luminosity of 2.9 pb^{-1}. The discrepancy one sees is due to the different ϵ_{HLT} in data and simulation.

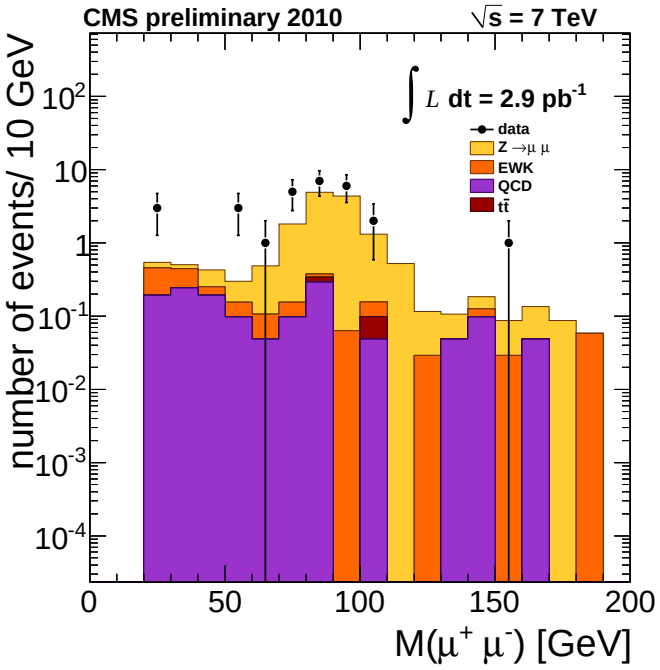

Figure 6: Invariant mass distribution of $Z_{\mu s}$ candidates for data and MC signal and background events for a luminosity of 2.9 pb^{-1}.

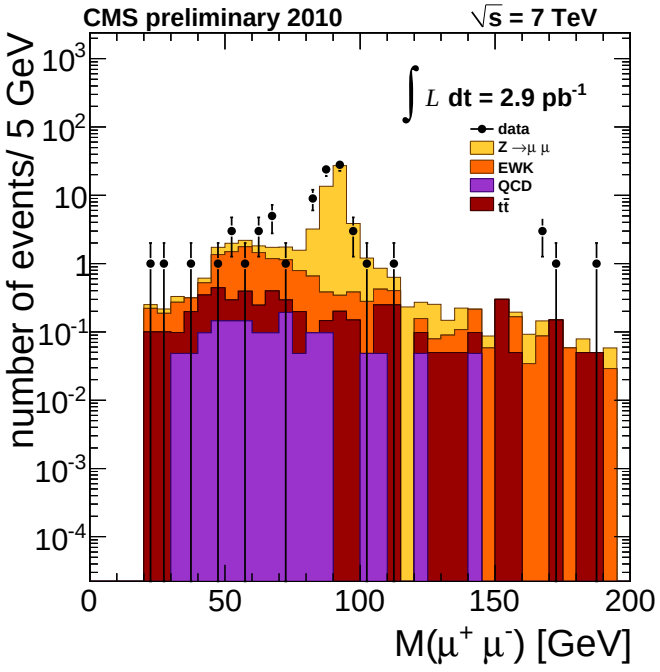

Figure 7: Invariant mass distribution of $Z_{\mu t}$ candidates for data and MC signal and background events for a luminosity of 2.9 pb^{-1}.

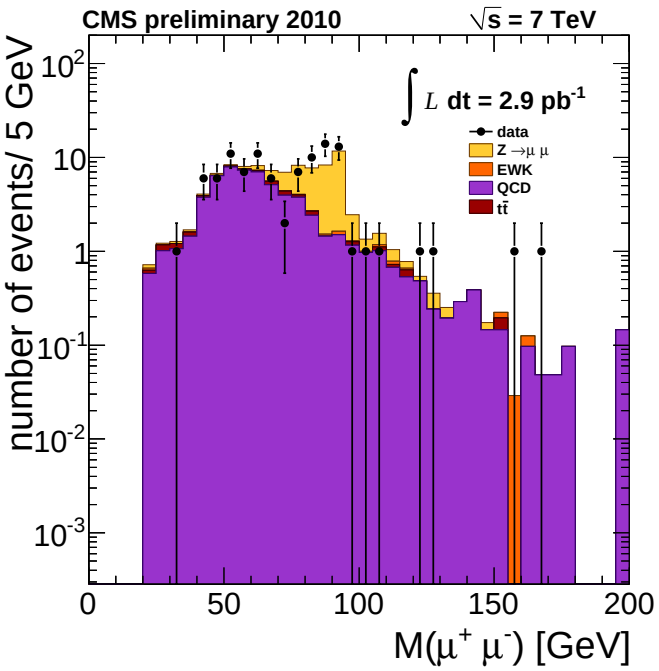

Figure 8: Invariant mass distribution of $Z_{\mu\mu}^{\text{non iso}}$ candidates for data and MC signal and background events for a luminosity of 2.9 pb^{-1}.

3.5 Fit results

We have performed the fit on the 2.9 pb^{-1} 7 TeV collision data. Figures 9-11 show the fit result superimposed to the histograms for the $Z_{\mu s}$, $Z_{\mu t}$, and $Z_{\mu\mu}^{\text{non iso}}$ samples. Table 5 reports the yield and efficiencies determined fro m the fit. They are compared to the results obtained by a fit performed using the the MC signal plus background only scaled to 2.9 pb^{-1}. In addition, the MC truth values of the average efficiencies, obtained from a sample of $Z \rightarrow \mu^+\mu^-$ MC signal events, are also reported in the Table. The resulting χ^2 and correspondent p-value (i.e. the probability of obtaining a value greater that the obtained one, evaluated from the χ^2 distribution) assures the goodness of the fit procedure.

From the fit results and the comparison with the MC-truth, one can see that all the efficiencies found in data agree quite well with the expectation (even tough slightly lower) with except of the trigger efficiency which is significant lower in data, as we can already see from the plots in Fig. 5 and 4, showing that the events in the $Z_{\mu\mu}^{\text{1HLT}}$ are visible more than the expectation and the contrary for the $Z_{\mu\mu}^{\text{2HLT}}$ category. This extra trigger inefficiency in data is however well know in the CMS community and some more plots, reasons and discussion will be given in the following section 3.10.

Given the low statistics, the polynomial degree of the background shape is truncated to the first order, and the $Z_{\mu s}$ histogram, wch containes only about 20 entries, is supposed to be background free (Table 3 shows that the background expected fraction is about 10%, not possible to subtract with such a low number of entries).

The correlation coefficients of the fit parameters is reported for completeness in Table 4. The first line of the matrix correlation table reports the correlations between the Z yield and the other fit parameter. No correlations greater than 13% are present.

An additional test is doing evaluating the poissonian likelihood ratio variation from the minimum versus the yield value (after fixing all the efficiency term parameter in the fit). This variation is compared to an ideal Gaussian parabolic shape as a function of the Z yield, where the σ of the Gaussian is fixed to the yield one standard deviation error around the best fit minimum. So we can safely consider a Gaussian approximation to evaluate the error of the fitted $Z \rightarrow \mu^+\mu^-$ yield. The comparison is shown in Fig. 12.

3.6 Kinematic acceptance

Once the $Z \rightarrow \mu^+\mu^-$ yield has been determined, we need to evaluate the kinematic acceptance at generator level in order to determine the cross-section in an enlarged kinematic region.

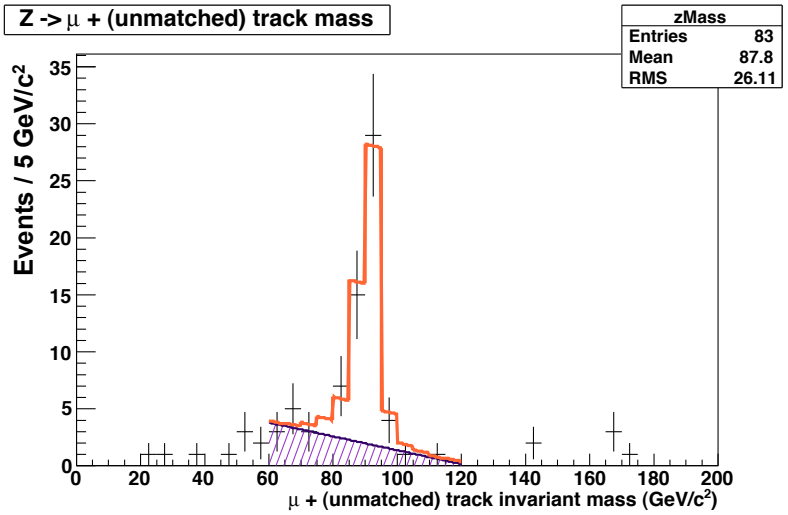

Figure 9: Fit curve superimposed to the invariant mass histogram of $Z_{\mu t}$ candidates for 2.9 pb^{-1} of LHC 7 TeV collision data.

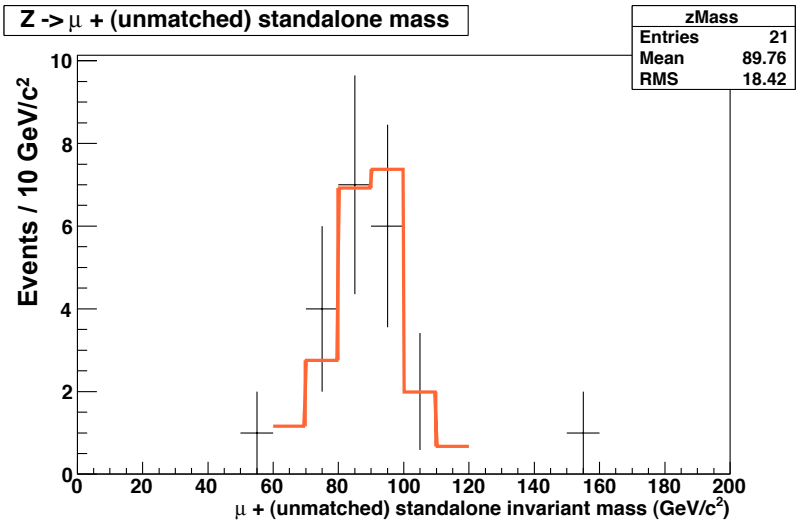

Figure 10: Fit curve superimposed to the invariant mass histogram of $Z_{\mu s}$ candidates for a sample corresponding to an integrated luminosity of 2.9 pb^{-1} of LHC 7 TeV collision data.

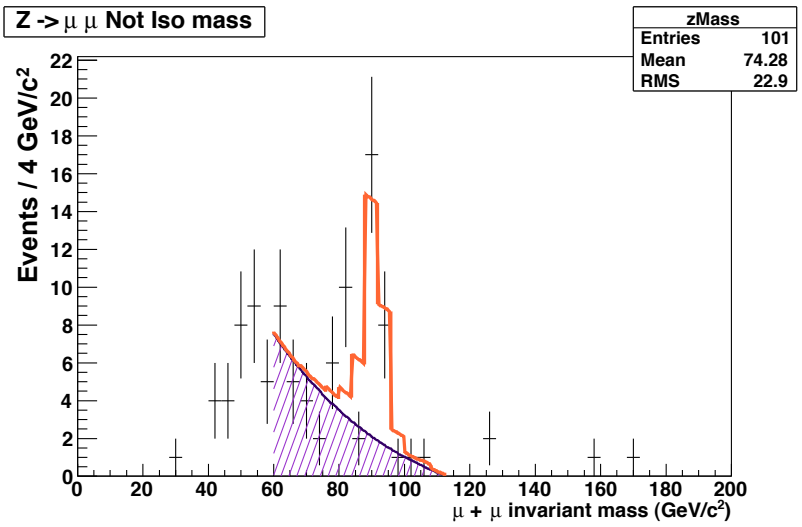

Figure 11: Fit curve superimposed to the invariant mass histogram of $Z_{\mu\mu}^{\text{non iso}}$ candidates for a sample corresponding to an integrated luminosity of 2.9 pb^{-1} of LHC 7 TeV collision data.

Param.	Description	1	2	3	4	5	6	7	8	9	10
Yield	$Z \to \mu^+\mu^-$ yield	1.000	-0.049	-0.126	-0.122	-0.081	-0.064	-0.055	0.036	0.052	-0.055
ϵ_{trk}	tracking efficiency	-0.049	1.000	0.029	0.017	0.032	0.000	0.000	0.000	0.000	0.000
ϵ_{sa}	standalone efficiency	-0.126	0.029	1.000	0.0024	0.045	0.000	0.177	-0.114	0.000	0.000
ϵ_{iso}	isolation efficiency	-0.122	0.017	0.024	1.000	0.000	-0.270	0.000	0.000	-0.220	0.231
ϵ_{HLT}	trigger efficiency	-0.081	0.032	0.045	0.000	1.000	0.000	0.000	0.000	0.000	0.000
α	background exponential slope	-0.064	0.000	0.000	0.270	0.000	1.000	0.000	0.000	-0.957	0.932
A_0	$Z_{\mu t}$ bkg polyn. 1^{st} degree term	-0.055	0.000	0.177	0.000	0.000	0.000	1.000	-0.978	0.000	0.000
A_1	$Z_{\mu t}$ bkg polyn. 2^{nd} degree term	0.036	0.000	-0.114	0.000	0.000	0.000	-0.978	1.000	0.000	0.000
B_0	$Z_{\mu\mu}^{\text{non iso}}$ bkg polyn. 1^{st} degree term	-0.052	0.000	0.000	-0.220	0.000	-0.957	0.000	0.000	1.000	-0.995
B_1	$Z_{\mu\mu}^{\text{non iso}}$ bkg polyn. 2^{nd} degree term	-0.055	0.000	0.000	0.231	0.000	0.932	0.000	0.000	-0.995	1.000

Table 4: Correlation coefficients of the fit parameters from the simultaneous fit minimization

$\int L\text{d}t = 2.9\text{pb}^{-1}$	fit results on data	simulation (2.9pb^{-1})	MC-truth ef ficiencies
ϵ_{HLT}	0.883 ± 0.008	0.930 ± 0.007	0.9319 ± 0.0014
ϵ_{iso}	0.985 ± 0.004	0.990 ± 0.004	0.9914 ± 0.0004
ϵ_{sa}	0.964 ± 0.004	0.971 ± 0.004	0.9724 ± 0.0006
ϵ_{trk}	0.994 ± 0.005	0.994 ± 0.004	0.9927 ± 0.0007
$N_{Z\to\mu^+\mu^-}$	1050 ± 35	1107 ± 37	
χ^2/ndof	1.074	1.034	
$p-$value	0.373	0.402	

Table 5: Comparison between fit parameters results with the fit model described in this chapter performed in data with simulation signal and background scaled to the data luminosity. χ^2/NDOF and p-value are also requested. MC-truth values of the average efficiencies are also shown for comparison.

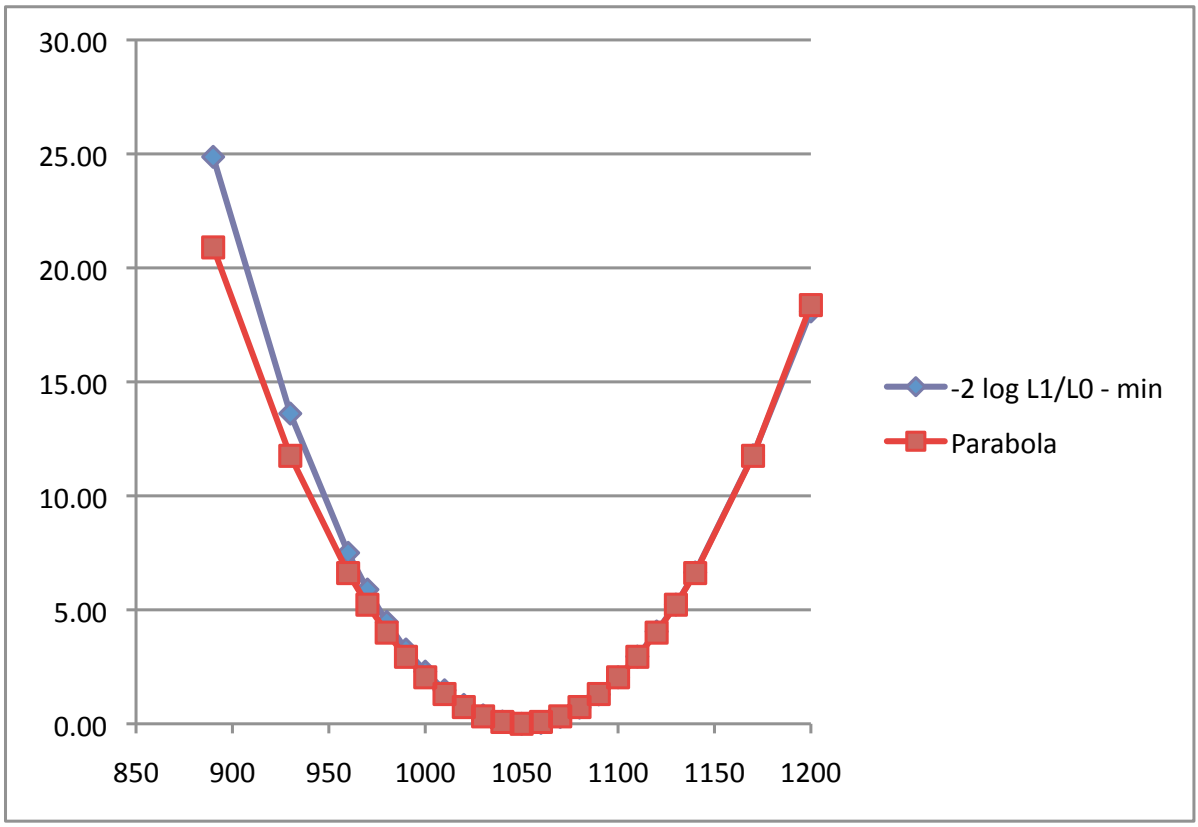

Figure 12: Poissonian likelihood ratio variation from the minimum versus the yield value compared with a Gaussian parabola.

The acceptance of the applied kinematic selection can be evaluated with Monte Carlo, and is somewhat sensitive to the generator adopted.

Aiming to determine the cross section in the same mass region used in the fit, but without any p_T and η cut the acceptance we need to correct is:

$$\epsilon^{\rm kin} = \frac{N(60 < m_Z < 120, p_{T,\mu} > 20, |\eta_\mu| < 2.1)}{N(60 < m_Z < 120)}, \tag{39}$$

where the numerator of the formula is the number of events considering muon after the final state radiation (because these are the muons we detect), while in the denominator the mass of the dimuon system is evaluated before the final state radiation. That is done in order to compare the final cross-section number with a theoretical prediction which includes also the final state radiation in the calculation.

Running on the MC $Z \rightarrow \mu^+\mu^-$ sample used for the analysis I found for the geometric acceptance the value is:

$$\epsilon^{\rm kin} = 0.3977 \pm 0.0017. \tag{40}$$

In order to use the Monte Carlo estimate, we need to verify that the acceptance estimated on generator particle and on reconstructed muons is identical and not affected too much from resolution effects. The good agreement has been verified in data with the statistics got so far and the relative systematics quoted as 0.2%.

3.7 Systematic Uncertianties

We can account for sources of systematics to the $Z \rightarrow \mu^+\mu^-$ cross-section measurement the followings:

- The first source of systematic uncertainty is the LHC machine luminosity estimate which amount to 11% [6] and will be quoted separately in the final number.
- A second source is the theoretical uncertainty which affect the acceptance, due to the uncertainties on parton density function. On top of higher order QCD corrections, an attempt has been carried on to estimate the effect of Electroweak diagrams not fully implemented in our baseline MC: final state radiation and virtual and non-virtual corrections. A complete list of results can be found in [11].
- A subtle source of systematics due to the on-line data taking, hence the L1 trigger, is the loss of muon events for trigger pre-firing, i.e. wrong assignment to the muon(s) bunch crossing number. This effect is due to wrong timing in the DT, CSC and RPC system, and is especially affecting the muon system overlap region ($0.9 < |\eta| < 1.2$) in which one should take care not only on the timing of the DT, CSC or RPC only, both also on the synchronization of the three subsystems. Anyway the correction to be applied for those timing problem has been estimated for the current data to be at maximum $1.0 \pm 0.5\%$ for the $Z \rightarrow \mu^+\mu^-$ channel. This estimate has been obtained searching events in which a standalone-standalone pair of muons, peaking at the Z mass value is found: muon pre-firing indeed role out the tracker system from the muon measurements, resuting in the impossibility to built a L3 muon online and a global muon in the offline reconstruction. We just remark that it is a global scale factor to the cross-section (to be enhanced by 1%, becuase we loss these 1% of events) and the 0.5% uncertainty is taken as systematic uncertainty.
- The remaining sources of systematics are then the one introduced with the fit procedure.

  We build the probability functions for the signal in a fully data driven way. The same is not true for the background shape, built as polynomial of first degree times an exponential. We tried to change the background from first to second degree polynomial functions, then to fix to zero the slope of the exponential and then vary the binning. The fit yield value is very stable. So we took half the difference between the max and min fitted yield, and we assigned it as systematic error. We estimate a 0.7% uncertainty due to this effect.

  The $Z_{\mu\mu}^{\rm 2HLT}$ and $Z_{\mu\mu}^{\rm 1HLT}$ histograms are supposed to be background free, but we know form MC that we have an irreducible contamination of less than 0.5% with the given selection. We added a flat background contribution to the two histograms and we saw that the fit yield output changes by an amount of $0.3 \times$ the backgorund over signal ratio. So we can quote as 0.2% as a conservative estimate of systematics error due to neglecting the background in the $Z_{\mu\mu}^{\rm 2HLT}$ and $Z_{\mu\mu}^{\rm 1HLT}$ histograms.

  Adding these two numbers in quadrature we can quote as a conservative estimate for the fit systematics of 1%.

Table 6 below reports all the contribution to the systematics uncertaities to the the data driven $Z \rightarrow \mu^+\mu^-$ cross-section measurement.

Table 6: Table of systematic uncertainties for the simultaneous fit $Z \rightarrow \mu^+\mu^-$ cross-section measurement.

Source	%
Trigger firing	0.5
Muon momentum scale/resolution	0.2
Fit Background shape and subtraction	1.0
PDF uncertainty in acceptance	1.2
Other theoretical uncertainties	1.6
TOTAL(without luminosity uncertainty)	2.3
Luminosity	11.0

3.8 cross-section determination

At this point all the ingredients to finally evaluate the $Z \rightarrow \mu^+\mu^-$ cross section with the first 2.9 pb^{-1} of 7 TeV collision data are available.

We start from the well known formula for the extraction of the cross-section already introduced in the Equation 1

As can be seen in Tab 3 the expected contamination of irreducible background, f_{bkg}, in the $Z_{\mu\mu}^{\rm 2HLT}$ and $Z_{\mu\mu}^{\rm 1HLT}$ categories is $f_{bkg} = 0.37\%$ (3.5 $\pm$ 0.3 events on a total of 950 expected signal events). [1)]

The simultaneous fit strategy gives directly the Yield corrected by the efficiencies to select the $Z \rightarrow \mu^+\mu^-$candidates, so we can evaluate the cross-section as:

$$\sigma = \frac{Y(1 - f_{bkg})}{A \int \mathcal{L} dt} \tag{41}$$

A 1% correction due to the loss of muon events due to trigger pre-firing in the first era of CMS data taking is also applied (as explained in Section 3.7). The following cross-sections for Z production is then measured:

$$\sigma(\mathbf{pp \rightarrow ZX}) \times \mathbf{BF(Z \rightarrow \mu^+\mu^-)} = \mathbf{0.924 0.031(stat.) 0.022(syst.) 0.101(lumi.) nb}, \tag{42}$$

The reported Z cross-sections is limited to the invariant mass range 60 ¡ m$_{\mu^+\mu^-}$ ¡ 120 GeV/c^2, and is corrected for the kinematic acceptance. The NNLO prediction for Z production is 0.97 $\pm$ 0.04 nb, so we find very good agreement with the Standard Model prediction.

3.9 correction factors for $W \rightarrow \mu\nu$ analysis

The $W \rightarrow \mu\nu$ selection requires the presence of an high p_T muon accompanied by a significant amount of missing transerve energy in the event.

For the first $W \rightarrow \mu\nu$ data driven measurement at CMS one needs to get the correction factor DATA/MonteCarlo (ρ_{eff}) for the efficiencies to reconstruct, trigger and identify a muon. That is done to correct the efficiencies taken directly from the simulation in a way similar to the one used in the first era of the $Z \rightarrow \mu^+\mu^-$ analysis, described in Section **??** . The correction value for the $W \rightarrow \mu\nu$ has been obtained by mean of the simultaneous fit to the $Z \rightarrow \mu^+\mu^-$ sample described in the note comparing the results obtained in data and simulation.

The muon selection in the $W \rightarrow \mu\nu$ analysis is equivalent to the one used for the $Z \rightarrow \mu^+\mu^-$ except for two additional requirements on the global muon track: the $\chi 2$ of the fit to be less than 10 and the requirement for the global muon to be also a tracker muon. We will denote as ϵ_{sel} the efficiency for the two additional cuts.

[1)] From the Table 3 also one can see that the QCD contribution to the background is very little w.r.t. other EWK channels and $t\bar{t}$. So we don't need to care for any possble increase of the QCD contribution w.r.t. to simulation where QCD (especially $b\bar{b}$) decay and punch-troughts in the muon system are not correctly simulated. This scale factor to apply to the QCD background has been anyway estimated to be not greater than 1.5. As we subtract the background in the other loose categories where the QCD is the main source of background, we don't need to consider this additional increment also for these histograms.

With the $Z \rightarrow \mu^+\mu^-$ selected events we can measured ϵ_{sel} as a ratio of di-muons from global-global pairs in the mass range with and without those cuts applied to both muons (having applied fisrt all the other cuts).

The measurements of $\epsilon_{\rm HLT}$, $\epsilon_{\rm iso}$, ϵ_{trk}, ϵ_{sa} on data and simulation has been already shown in table 5. Now we show the resulting correction factors and the numerical values of ϵ_{sel}. The total correction factor ρ_{eff} is the product of all the corrections. A summary of the results is given in Table 7.

Efficiency	Data	Simulation	Data/Simulation(ρ_{eff})
$\epsilon_{\rm HLT}$	0.883 ± 0.008	0.9319 ± 0.0014	0.947 ± 0.009
$\epsilon_{\rm iso}$	0.985 ± 0.004	0.9914 ± 0.0004	0.994 ± 0.004
ϵ_{sa}	0.964 ± 0.004	0.9724 ± 0.0006	0.992 ± 0.005
ϵ_{trk}	0.994 ± 0.005	0.9927 ± 0.0007	0.998 ± 0.003
ϵ_{sel}	0.997 ± 0.003	0.9967 ± 0.0005	1.0 ± 0.003
Net(W)	0.828 ± 0.011	0.8874 ± 0.0013	$\mathbf{0.933 \pm 0.012}$

Table 7: Final efficiency factors used in the $W \rightarrow \mu\nu$ analysis. There were obtained applying the simultaneous fit technique on a clean $Z \rightarrow \mu^+\mu^-$ sample.

As can be seen in the table, most of the correction numeric values are very close to unity. Only the trigger efficiency is about 5% lower in data than in simulation, a fact that has been confirmed many times in CMS and will be discussed in the next Section.

Subset	Data/Simulation(Net ρ_{eff})
positive muons	0.935 ± 0.018
negative muons	0.931 ± 0.019
barrel ($\|\eta\| < 0.9$)	0.955 ± 0.024
transition (0.9 ¡ $\|\eta\| < 1.2$)	0.89 ± 0.04
endcap (1.2 ¡ $\|\eta\| < 2.1$)	0.92 ± 0.03

Table 8: Correction factors for subsets of muons

Additional studies performed with the $Z \rightarrow \mu^+\mu^-$selection and analysis strategy essential for the $W \rightarrow \mu\nu$analysis one are the following:

- We evaluated the correction factors for positive and negative muons separately, as shown in Table 8. The difference amounts to 0.4% and is compatible with zero. Hence the same correction can be applied for the $W^+ \rightarrow \mu^+\nu$ and $W^- \rightarrow \mu^-\nu$ and in the ratio W^+/W^-.
- The table also lists the correction values for the barrel, endcap and transition regions of the muon system. The correction factors are fairly uniform with perhaps a somewhat lower value in the transition, or overlap region between the DTs and the CSCs.
- Another important result found is the global correlation between the product of the efficiencies for the muon selection and the $Z \rightarrow \mu^+\mu^-$ yield. This number is used for the error propagation in the W over Z ratio, which is one of the most important EWK measurement ..... This value has been obtained from the simultaneous fit described above reparametrizing one of the efficiency as $\epsilon_{tot} = \epsilon_{\rm HLT}\epsilon_{trk}\epsilon_{sa}\epsilon_{\rm iso}$, and introducing this parameter in the fit minimization. The total correlation found is

$$correlation(Yield, \epsilon_{tot}) = -0.236 \tag{43}$$

3.10 Trigger efficiency estimate using $Z \rightarrow \mu^+\mu^-$

Dimuon resonance such as J/Ψ, $\Upsilon(1s)$, Z are used to study the detector reconstruction, isolation and trigger efficiencies using the so called "Tag and Probe" method. This method, which has been successfully used in some form or another by past and present experiments, relies upon $Z \rightarrow \mu^+\mu^-$ decays to provide an unbiased, high-purity, muon sample with which to measure the efficiency of a particular selection cut, including the trigger. With the intention to study the trigger efficiency, a single muon trigger sample is used, from which a subset of di-muon events are selected. One of the muons, the "tag", is required to pass stringent muon identification criteria in order to have as low background as possible, while the other muon, the "probe", is only required to pass a set of identification criteria depending on the efficiency under study. The invariant mass of the tag and probe muon candidates is required to be within a window around m_Z . The tight criteria imposed on the tag coupled to the invariant mass requirement is sufficient to ensure high muon purity.

This method has been applied to study the muon trigger efficiency, to study the single muon trigger selection path named `HLT_Mu9`. Both tag and prob muons are required to pass stringent identification and isolation cuts (see Section **??**), in order to provide the efficiency to be used for the $W \rightarrow \mu\nu$ analysis. Hence the probe muon is required to pass these tight identification and isolation cuts and the trigger firing is investigated.

Applying this method we find for the average efficiency for $p_T > 20\ GeV/c$ and $|\eta| < 2.1$ in the first 2.9 pb^{-1} of collision data the value reported in Table 9 and in the plots of Fig. 13 and 14. For comparison we report also the efficiency we expect from the simulation, using the MC $Z \rightarrow \mu^+\mu^-$ simulated sample used in the note. As already remarked the correction we found to be applied to pass from simulated MC to data efficiency is of the order of 95%, to be precise 0.947 ± 0.008 for these tight selected muons.

The CMS community is investigating the reason of this 5% of extra inefficiency in data. As can be seen by the numbers and plots it is clear that the region much affected by thus trigger lost is the barrel-endcap overlap region ($0.9 < |\eta| < 2.1$), due to syncronization problem between DT, CSC and RPC detectors. It has been found that all these subsystem need to better calibrate their timing constants. That calibration can be done when more collision data will be available and so it is expected that the L1 trigger efficiency will increase in the near future.

In addition a second loss of efficiency has been found to be introduced in the L2 and L3 step, expecially in the endcaps, due to a probability some per cent higher than expected to assign a wrong charge to the muon in the L2-L3 steps. For that reason new L3 algorithms will be soon deployed on-line.

Table 9: Table of muon single muon trigger efficiency versus η obtained in data using the tag an prob method on $Z \rightarrow \mu^+\mu^-$ selected event.

	overall (—eta—¡2.1)	barrel ($\|\eta\| < 0.9$)	transition region (0.9¡ η¡1.2)	endcaps ($1.2 < \|\eta\| < 2.1$)
$Z \rightarrow \mu^+\mu^-$ MC	0.9333 ± 0.0010	0.9607 ± 0.0012	0.871 ± 0.003	0.920 ± 0.002
data (2.9 pb^{-1})	0.884 ± 0.007	0.934 ± 0.009	0.75 ± 0.03	0.871 ± 0.014
scale factor (data/MC)	0.947 ± 0.008	0.972 ± 0.010	0.86 ± 0.04	0.947 ± 0.017

4 EWK results.....

4.1 Additional categories to check the background

samecharge, 1 and 2 not iso ?????????? metterlo?????

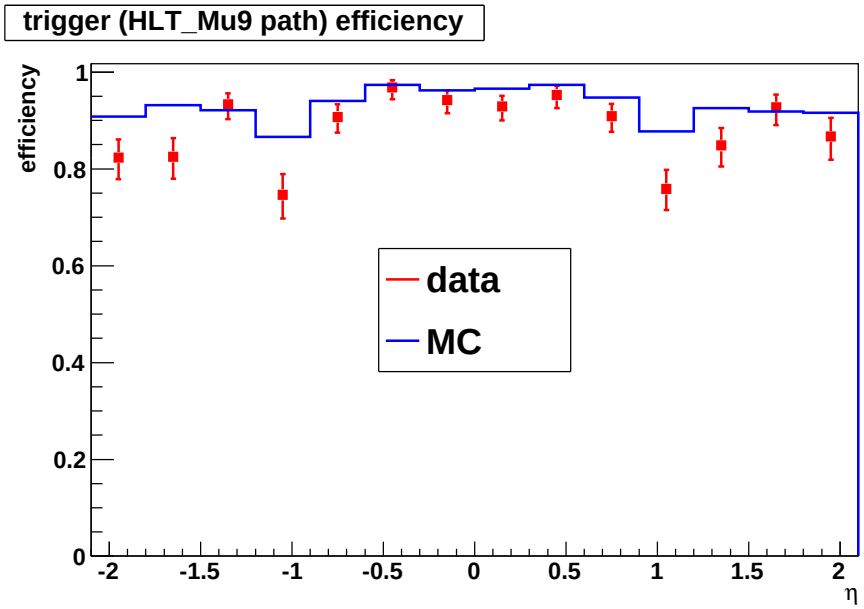

Figure 13: Muon single muon trigger efficiency versus muon η, obtained using tag and prob method on $Z \rightarrow \mu^+\mu^-$ selected events on 2.9 pb^{-1} of LHC 7 TeV collision data.

5 Luminosity measurement using W and Z

The machine luminosity monitor and measurement is one of the most important thing to assess in the first years of data taking of a new accelerator and through-tout its whole life.

The integrated luminosity in CMS is based on signals from the Forward Hadronic Calorimeter. Two methods for extracting a real-time relative instantaneous luminosity are used. The "zero counting," method in which the average fraction of empty towers is used to infer the mean number of interactions per bunch crossing. The second method exploits the linear relationship between the average transverse energy per tower and the luminosity. The choice of the online algorithm chosen to report the luminosity summary might get adjusted based on the data integrity/reliability namely the statistical uncertainty or systematics uncertainty due to the Forward Calorimeter or the background sensitivity. The different algorithm agree to within 5% so far. The final normalization of the luminosity is based on Van der Meer scans, which determine the size of the colliding beams and thus the luminosity with minimal reliance on simulation This techique was first pioneered by Van Der Meer at the ISR. See reference [12], article to which I contributed, for a review of the luminosity measurement issue at LHC, and [6] for a details on the CMS measurement systematic uncertainties.

The resulting measurement is the most reliable one and the recommended to be used for data analysis and is stored run by run (to be more precise lumisection by lumisections, where the lumisections is the smallest part of a CMS run lasting 23 s) in the CMS Condition Database and is accessible by the whole CMS community.

As already said the current precision of this method, resulting in a systematics for all cross-section measurement is 11% . The uncertainty associated to this measurement is supposed to lower in with the passing of the time, when all the LCH fill beam information will be calibrated and measured always better, but is eventually limited by the uncertainty on the knowledge of all the QCD processes contributing to the very forward physics.

Several offline method have been used in the first era of the LHC: above all the primary vertexes counting. The method counts the primary vertices falling in each lumisections and knowing the expectation for the theory manage to obtain a luminosity value for the lumisections. As the on-line HF method also the vertex counting is dominated finally by the QCD physics uncertainties.

With high integrated luminosity we can exploit EWK channels, once the Standard Model cross-section value will be definitely confirmed, to use them as luminosity monitor and eventually to measure the luminosity with low systematics. Muon decays are for sure more feasible for such a use, because in general CMS reaches better muon reconstruction and identification than electrons. As already seen in the previous Section already with about 3 pb^{-1} we have a measurement of the $Z \rightarrow \mu^+\mu^-$ cross section in which the systematical error is comparable with the

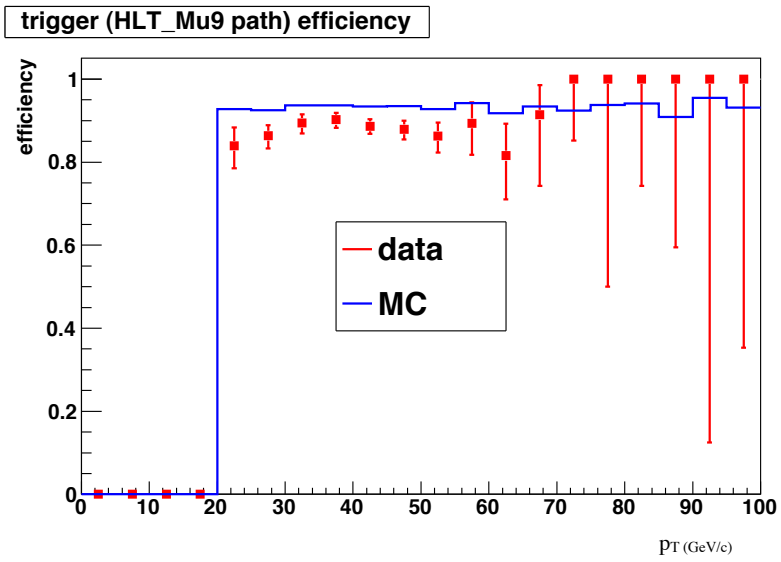

Figure 14: Muon single muon trigger efficiency versus muon p_T obtained using tag and prob method on $Z \rightarrow \mu^+\mu^-$ selected events on 2.9 pb^{-1} of LHC 7 TeV collision data.

statistical error, and it is neglecteble for the $W \rightarrow \mu\nu$ channel, with has about ten times graeter cross-section.

Already in the future year of the machine, when the instantaneous luminosity will reach the value of $L = 10^{33}\mathrm{s}^{-1}\mathrm{cm}^{-2}$ we will collect in less then 10 hours (hence a CMS run) an integrated luminosity of the order of the pb^{-1}, and when the luminosity will reach the design value of $L = 10^{34}\mathrm{s}^{-1}\mathrm{cm}^{-2}$ W and Z bosons decaying into muons will be produced with the rate of 10 and 1 Hz respectively.

Given that, we found very useful to develop a tool, inserted in the offline DQM framework, that counts the number of selected $W \rightarrow \mu\nu$ and $Z \rightarrow \mu^+\mu^-$ events and publishes them on a web page.

The software program is run centrally with the complete DQM offline chain producing the histogram containing the $Z \rightarrow \mu^+\mu^-$ mass and $W \rightarrow \mu\nu$ transverse mass distribution. A subsequent script developed also by myself access the web repository where this histograms are saved, counts the entries and applies the data driven method discribed in the previous Section and determine the integrated luminosity (assuming that the Standard Model cross-section).

This tool has been put in place already with the first runs and shows to agree well with the on-line measurements. We wait a larger instantaneous luminosity to better exploit its utility with the resulting small uncertainties.

A snapshot of the $W \rightarrow \mu\nu$ and $Z \rightarrow \mu^+\mu^-$ counting web page is shown in Figure 15

References

[1] N. Adam *et al.*, Towards a measurement of the inclusive $W \rightarrow \mu\nu$ and $Z \rightarrow \mu^+\mu^-$ cross sections in pp collisions at $\sqrt{s} = 14$ TeV, *CMS AN-2007/031* .

[2] M. De Gruttola *et al.*, Determination of the $pp \rightarrow ZX \rightarrow \mu^+\mu^-X$ inclusive cross section with a simultaneous fit of Z yield and muon reconstruction efficiencies, *CMS AN-2008/062* .

[3] M. De Gruttola *et al.*, Determination of the $pp \rightarrow ZX \rightarrow \mu^+\mu^-X$ inclusive cross section with a simultaneous fit of Z yield, muon reconstruction efficiencies and High Level Trigger efficiency *CMS AN-2009/005* .

[4] http://www.ichep2010.fr/.

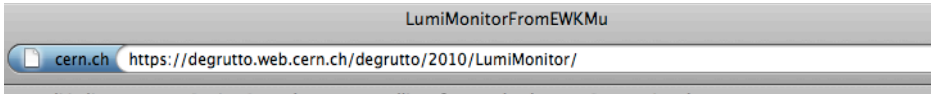

Luminosity expectation counting W and Z into muons (using dqm minimum bias(may27rerec run2010/Mu prompt-reco), assuming B/S = 10% for W and 1% for Z; disclaimer:all numbers

run	LumiFromWmn(nW*0.24) 1 / nb	LumiFromZmm(nZ*3.0) 1 / nb
143827	140.16	144.0
143831	12.48	6.0
143833	125.04	147.0
143835	30.48	24.0
143953	106.32	123.0
143954	31.92	33.0
143955	14.16	6.0
143956	7.68	3.0
143957	29.04	18.0
143959	17.28	33.0
143960	13.68	24.0
143961	52.32	54.0
143962	52.56	51.0
143977	0.0	0.0
144010	19.44	27.0
144011	78.24	78.0
144083	0.0	0.0
144086	64.56	63.0
144089	247.92	294.0
144112	280.8	285.0
144114	9.84	12.0
tot	3225.36+/-27.8	3312.0+/-99.7

Figure 15: Snapshot of the web page produced with the offline luminosity measurement tool using W and Z bosons decaying into muons. The numbers are in nb^{-1}.

[5] GEANT4 Collaboration, S. Agostinelli et al., GEANT4: A simulation toolkit, Nucl. Instrum. Meth. A506 (2003) 250303.

[6] CMS Collaboration, "Measurement of CMS luminosity", CMS PAS EWK-2010-004 (2010).

[7] CMS Collaboration, "Measurements of Inclusive W and Z Cross Sections in pp Collisions at $\sqrt{7}$ TeV", CMS PAS EWK-2010-002 (2010).

[8] Clopper, C.; Pearson, E. S. (1934). "The use of confidence or fiducial limits illustrated in the cas e of the binomial". Biometrika 26: 404-413.

[9] S. Baker and R. Cousins, Clarification of the Use of Chi-Square and Likelihood Functions in Fits to Histograms, NIM 221:437 (1984)

[10] J. Campbell and R.K. Ellis, Monte Carlo for FeMtobarn processes, 1449 http://mcfm.fnal.gov/.

[11] CMS Collaboration, "Updated Measurements ofInclusiveW and Z Cross Sections at 7 TeV", CMS AN-2010-26 4

[12] "Luminosity measurements at LHC". S. de Capua, (CERN) , F. Ferro, (INFN, Genoa) , M. De Gruttola, (I NFN, Naples) , M. Villa, (INFN, Bologna) . 2008. 12pp. Prepared for 5th Italian Workshop on LHC Physics (In Italian), Perugia, Italy, 30 Jan - 2 Feb 2008. Published in Nuovo Cim.123B:423-434,2008.